Article

Real-Time Power System Optimization Under Typhoon Weather Using the Smart "Predict, Then Optimize" Framework

Haoran Zhang * and Haoran Liu

School of Science and Engineering, The Chinese University of Hong Kong, Shenzhen 518172, China; haoranliu1@link.cuhk.edu.cn
* Correspondence: haoranzhang4@link.cuhk.edu.cn; Tel.: +86-192-0270-8138

Abstract: With the increase of extreme weather events caused by global climate change, the issue of power system resilience has become more and more important. Traditional power system management methods cannot cope with dynamic real-time changes, and it is difficult to effectively predict and respond to potential failures caused by extreme weather. To this end, this paper proposes a real-time power system optimization method based on the Smart "Predict, then Optimize" (SPO) framework. The SPO method first uses the Transformer model to predict, in real time, the future line damage states and then dynamically adjusts the optimization strategy based on the prediction results. This method can efficaciously enhance the prediction accuracy of faulty lines under extreme weather conditions and optimize generation scheduling, load management, as well as EV battery scheduling to minimize the system cost. This study proposes a solution based on the SPO loss function, artificial intelligence prediction model, and bi-level optimization model to address the dynamic optimization of power systems under extreme conditions, significantly enhancing the system's response to extreme weather events. The experimental results demonstrate that the SPO method can optimize system operation in real time, significantly reducing load shedding and total system cost during typhoon weather, which not only improves the system's economic efficiency but also effectively enhances power system resilience.

Keywords: optimization; SPO; transformer; extreme weather; system resilience

1. Introduction

With the intensification of global climate change, extreme weather such as storms, freezing rain and strong winds occur frequently, posing severe challenges to the stability and reliability of the power system [1]. Especially in typhoon weather, wind loads significantly increases the risk of transmission line failures, which may have a serious impact on large-scale users [2,3]. In 2012, Hurricane Sandy caused severe damage to the power system in several coastal states, leaving more than 8.5 million customers without power, lasting for weeks or even months in some areas [4,5]. However, the traditional power system management methods are difficult to deal with these complex fluctuations and extreme conditions, which is easy to cause chain failures or large-scale power outages, and cannot effectively predict and mitigate potential problems [6,7].

In typhoon disasters, serious accidents often occur in power grids due to transmission line damage probability. Analysis and prediction of transmission lines damage probability are of great significance for disaster prevention and reduction [8]. In recent years, in order to improve the resilience of power systems under extreme weather, many optimization

techniques have emerged. Based on the predicted loss state of the power system line, the load loss can be effectively reduced and the stability of the power system can be improved by scheduling generator start–stop, energy storage, EV charging and discharging in advance. However, more accurate predictions do not necessarily lead to better decisions [9,10]. Machine learning methods are often designed to minimize prediction errors, regardless of how the predicted results are used in subsequent optimization problems [11]. Reference [12] proposes a decision-oriented SPO loss function and SPO framework, which can improve the prediction model and make it better meet the system objectives under the condition of similar accuracy.

Due to the limited data of historical extreme events [13], a probability formula for calculating the relationship between wind speed and line damage was proposed in the literature [14,15] to generate a vulnerability curve for measuring the impact of typhoons on transmission or distribution networks. Based on the above theories, this paper conducted Monte Carlo simulation to generate a large amount of training data, including wind speed, the angle between the line and the direction around the typhoon, and the distance between the line and the typhoon center [16]. In addition, the Transformer model is used to predict the line state, the long-distance dependencies and global features in the time series are extracted by the encoder, and the sequential relationship between time steps is captured by the position encoding. The model inputs multiple variables at each time step as a whole, uses the self-attention mechanism to model the complex relationship between variables and time steps, and finally realizes classification prediction through the fully connected layer [17].

This paper proposes a bi-level optimization model based on SPO framework to solve the upper problems. The SPO method first predicts the real-time line damage state through the Transformer model, and then makes optimization decisions based on the prediction results, thereby dynamically scheduling power system resources to reduce load reduction as much as possible [18,19]. At the same time, the upper model aims to minimize the total cost of the power system, while the lower model aims to maximize the economic profit of EV owners [20,21].

The main contributions of this paper are summarized as follows:

1. **The combination of SPO framework and reinforcement learning**: The SPO framework is combined with reinforcement learning for the first time, and the scheduling error is reduced through the policy gradient optimization method, which improves the accuracy of fault protection and cost control.
2. **Design of bi-level optimization structure**: A bi-level structure including upper and lower optimization is proposed. In the upper layer, the optimal scheduling decision was generated according to the predicted line state to minimize the total system cost. The lower layer aims at the Electric Vehicle (EV) energy storage system to maximize the economic benefits of EV owners.
3. **Transformer model is applied to power system resilience analysis**: Due to the randomness and timing characteristics of the outage process in extreme weather, this paper uses Transformer model for fault prediction, and simulates it by Monte Carlo Simulation (MCS) method. Combined with SPO loss function, the decision optimization is successfully realized.

The remainder of this paper is organized as follows: Section 2 introduces the Line Failure Probability Model; Section 3 outlines the Framework and Feedback Adjustment Mechanism; Section 4 presents the objectives and constraints; Section 5 discusses the case studies; and Section 6 provides the conclusions.

2. Line Failure Probability Model

In extreme weather conditions, such as winter storms, factors such as damage to power system lines and power flow shifts may lead to grid line failures, thereby causing changes in system states. The operating status of power grid lines under winter storm conditions can be expressed by the following formula:

$$u_{l,i,t}^{\mathrm{F}} = \begin{cases} 1, & \text{line is operating normally} \\ 0, & \text{line is in failure} \end{cases}$$

where $u_{l,i,t}^{\mathrm{F}}$ indicates the operational state of power grid line l at time t; 1 indicates normal operation, and 0 indicates a fault.

As the winter storm develops and moves, it impacts transmission lines along its path, resulting in sequential and random changes in the system state over time. By discretizing the continuous changes of the system state, the fault evolution process can be simulated. Moreover, since the system state depends only on the previous state, the state transition process can be regarded as a discrete-time Markov process. The transition probability between two adjacent time periods can be expressed as

$$Pr(u_{l,i,t}^{\mathrm{F}}, u_{l,i,t+1}^{\mathrm{F}}) = \prod_{j \in \Omega_{t+1}^{\mathrm{F}}} Pr(u_{l,j,t}^{\mathrm{F}}, u_{l,j,t+1}^{\mathrm{F}}), \quad i \in \Omega_t^{\mathrm{F}}$$

where $u_{l,i,t}^{\mathrm{F}}$ represents the system's state at time period t; $\Omega_{t+1}^{\mathrm{F}}$ is the set of grid lines that may fail in period $t+1$, and Ω_t^{F} represents the set of system states at time t; $Pr(u_{l,j,t}^{\mathrm{F}}, u_{l,j,t+1}^{\mathrm{F}})$ denotes the probability of a grid line's state transitioning from $u_{l,j,t}^{\mathrm{F}}$ to $u_{l,j,t+1}^{\mathrm{F}}$.

In this study, we used an IEEE 57-node power system combined with Monte Carlo simulations to generate a large dataset to simulate the effects of extreme weather on power systems. The generated data covers the wind speed distribution of the line, the failure rate, and the status of the line if it is damaged.

To predict line failure, we designed a prediction model based on Transformer. We choose the Transformer to process time series data for each line. Through a self-attention mechanism, it is able to capture global dependencies between different time steps, allowing the model to model complex time series data more efficiently. In addition, Transformer incorporates location coding to ensure that the model understands the sequential nature of the data. After processing by multi-layer encoders, the model gradually enhances the abstract understanding of the input data to generate high-level feature representations for classification.

In order to show the superiority of our SPO loss function, we compare the cross-entropy loss with the SPO loss function. Cross-entropy loss is often used to solve the class imbalance problem, which can effectively improve the classification accuracy. The SPO loss function can not only optimize the model performance but also reduce the total operating cost of the system more effectively. Specifically, the SPO approach combines forecasting with optimization to dynamically adjust the scheduling strategy of a power system, further reducing the frequency of failures and reducing operating costs.

3. Framework and Feedback Adjustment Mechanism

In this study, we use the IEEE 57-node power system and Monte Carlo simulations to generate a large dataset. These dataset models the effects of extreme weather on the power grid, including wind speed distribution, failure rates, and line damage states.

1. **Data generation.**
   Large data sets are generated through Monte Carlo simulations, including the wind speed distribution of the line, the failure rate, and the operating status of the line (whether it is damaged or not).
2. **Feature extraction and temporal processing.**
   Use Transformer to process time series data for each line, capture time dependencies, and efficiently construct sequential features to fully characterize the dynamic characteristics of the line.
3. **Classification and high-level feature representation.**
   A multilayer encoder is used to generate a high-level feature representation for classification.
4. **Feedback adjustment and strategy optimization (SPO and reinforcement learning).**
   The SPO framework is combined with reinforcement learning to adjust line failure state prediction errors and minimize operating costs due to scheduling deviations. The specific process is as follows:

   - **Problem definition.**
     Scheduling decisions are based on the predicted line state and the corresponding optimal cost and scheduling decisions obtained through a two-tier optimization model: $\hat{c}^T w^*(\hat{c})$, where $\hat{c}$ represents the predicted cost vector, and $w^*(\hat{c})$ represents the optimal scheduling decision under the predicted cost. Prediction bias is measured by applying the predicted decision to the actual line state to obtain the actual cost $c^T w^*(\hat{c})$ and comparing it with the true optimal cost $c^T w^*(c)$. Based on these two values, we define the SPO loss function as $\delta_{total} = c^T w^*(\hat{c}) - c^T w^*(c)$.

   - **Reinforcement learning and policy gradient optimization.**
     The total loss δ_{total} is the difference between the predicted total cost and the actual total cost as a feedback signal in the optimization process. This allows us to quantify the impact of prediction errors on the total cost of system scheduling. The loss is then distributed according to the difference between the actual current flow and the optimal current flow for each line. A line with a large current difference will incur more losses, while a line with a zero current difference will not incur losses. This allocation method can accurately reflect the impact of each line on the system scheduling, and help optimize scheduling decisions.
     The δ of each line is converted into a reward. To minimize loss δ, reinforcement learning defines a reward as

     $$reward = -\frac{1}{\exp(-\delta) + \xi},$$

     where ξ is a small constant number. To maximize this reward, we use the policy function $\pi_\theta(a|s)$ to express the probability of choosing an action a in a given state s, where θ is the parameter of the policy. The parameter θ is updated using the policy gradient method to maximize the expected reward, thereby minimizing δ. The specific steps are as follows:

     – **Prediction and action selection**: for a given state s (e.g., characteristics of a line), the model outputs an action a (i.e., the predicted line state) and generates a scheduling decision.
     – **Actual cost evaluation**: the predicted decision is applied to the actual state to calculate the actual cost $c^T w^*(\hat{c})$.
     – **Loss calculation and policy gradient update**: According to the policy gradient formula,

$$\nabla_\theta J(\theta) = \mathbb{E}[Q^{\pi_\theta}(s,a)\nabla_\theta \log \pi_\theta(a|s)]$$

where $\log \pi_\theta(a|s)$ is the gradient of the action's probability with respect to θ, and $Q^{\pi_\theta}(s,a)$ represents the expected cumulative discounted reward obtained by taking action a in state s and following policy π_θ thereafter. This update optimizes future scheduling decisions.

5. **Loss function comparison and conclusion.**
The experimental results show that SPO loss combined with reinforcement learning significantly improves the efficiency of the system compared with cross-entropy loss. Compared to traditional methods, SPO losses significantly reduce total system costs through dynamic feedback and policy optimization, demonstrating strong advantages in predicting the impact of extreme weather on the grid.

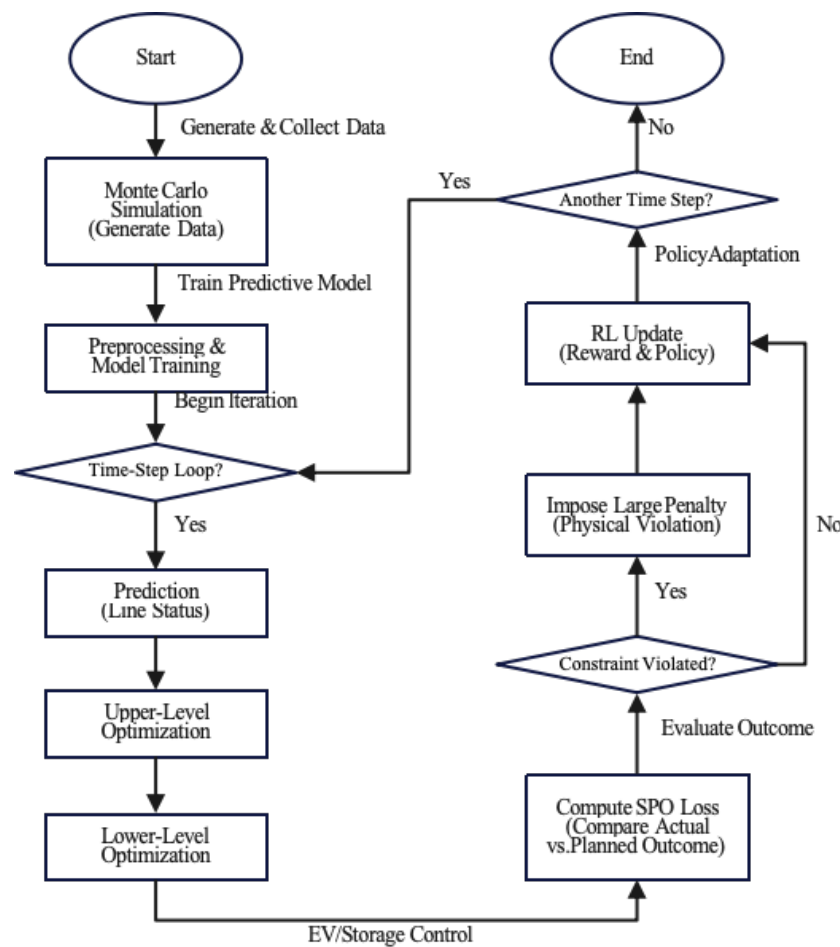The specific experimental process is shown in Figure 1 below.

Figure 1. Bi-level optimization decision process for power system based on SPO framework.

4. Objective and Constraints

The objective of the upper layer problem is to minimize the total operating cost of the power system by optimizing the resource allocation and operation modes of the system. This objective function covers the costs of generation, the costs of starting and stopping generators, the costs of load reduction, the costs and benefits of energy storage system charging and discharging, and the costs of charging electric vehicles (EVs).

$$\min \sum_{t \in \mathcal{T}} \left(\sum_{g \in \Omega_G} C_G^S P_{g,t}^G + C_{SU} u_{g,t} + C_{SD}(1 - u_{g,t}) \right.$$
$$+ \sum_{b \in \Omega_B} C_P^S P_{b,t}^S + \sum_{m \in \Omega_b^{\mathcal{M}}} C_m^{S,C} P_{m,t}^{S,C} - C_m^{S,D} P_{m,t}^{S,D}$$
$$\left. + \sum_{q \in \Omega_b^{EV}} C_t^{EV} P_{q,t}^{EV,C} \right) \tag{1}$$

The first part, $\sum_{t \in \mathcal{T}} \sum_{g \in \Omega_G} C_G^S P_{g,t}^G$, describes the total generation cost of all generators over the entire scheduling period. Here, $\mathcal{T}$ is the set of time periods, representing the scheduling problem's involvement in all time steps; Ω_G is the set of generators, containing all generators in the system; C_G^S is the unit power generation cost, expressed in yuan (CNY) per kilowatt; and $P_{g,t}^G$ is the generation power of generator g at time t, expressed in kilowatts. By weighted summing the generation power of all generators at all time periods, the total generation cost can be obtained.

The second part, $\sum_{t \in \mathcal{T}} \sum_{g \in \Omega_G} \left(C_{SU} u_{g,t} + C_{SD}(1 - u_{g,t}) \right)$, delineates the startup and shutdown costs of generators. Herein, C_{SU} represents the startup cost of the generator, quantified in yuan (CNY); C_{SD} stands for the shutdown cost of the generator, likewise quantified in yuan (CNY); and $u_{g,t}$ constitutes a binary variable denoting the operating status of generator g at time t. If the generator is in the startup mode, then this part calculates the total startup and shutdown cost for the entire cycle by weighted summing the generator's startup and shutdown behavior for all time periods.

The third part, $\sum_{t \in \mathcal{T}} \sum_{b \in \Omega_B} C_P^S P_{b,t}^S$, represents the penalty costs for load reduction. Herein, Ω_B constitutes the set of grid nodes (i.e., buses), and C_P^S is the penalty cost per unit load reduction, expressed in yuan (CNY) per kilowatt. $P_{b,t}^S$ is the load reduction power at node b at time t, also expressed in units of kilowatts. The total economic loss resulting from load reduction is obtained via weighted summation of the load reduction quantities for all nodes and all time periods.

The fourth part, $\sum_{t \in \mathcal{T}} \sum_{m \in \Omega_b^{\mathcal{M}}} \left(C_m^{S,C} P_{m,t}^{S,C} - C_m^{S,D} P_{m,t}^{S,D} \right)$, delineates the cost and revenue associated with the charging and discharging of the energy storage system. Here, $\Omega_b^{\mathcal{M}}$ constitutes the set of energy storage systems; $C_m^{S,C}$ represents the unit charging cost of energy storage device m, measured in yuan (CNY) per kilowatt; $C_m^{S,D}$ denotes the unit discharging revenue of energy storage device m, measured in yuan (CNY) per kilowatt; $P_{m,t}^{S,C}$ is the charging power of energy storage device m at time t, measured in kilowatts; and $P_{m,t}^{S,D}$ is the discharging power of energy storage device m at time t, also measured in kilowatts. By calculating the charging cost and discharging revenue of the energy storage system for all time periods, the economic impact of the energy storage system within the scheduling period can be evaluated.

The fifth part, $\sum_{t \in \mathcal{T}} \sum_{q \in \Omega_b^{EV}} C_t^{EV} P_{q,t}^{EV,C}$, is the overall cost of charging electric vehicles. Here, Ω_b^{EV} is the set of electric vehicles on bus bar b; C_t^{EV} is the unit electricity price of electric vehicles at time t, measured at yuan per kilowatt-hour; and $P_{q,t}^{EV,C}$ is the charging power of electric vehicle q at time t, measured in kilowatts. The total cost of charging electric vehicles can be got through the weighted summation of the charging power of all electric vehicles during the scheduling period.

The objective function is to minimize the total operating cost of the power system by optimizing the resource allocation and operation modes in the system, balancing the economic costs related to generation, startup and shutdown, load curtailment, energy storage operation, and electric vehicle charging, and ensuring the economic efficiency and operational performance of the system.

4.1. Constraints of the Power System

$$\sum_{g\in\Omega_G} P_{g,i,t}^G + \sum_{q\in\Omega_b^{EV}} P_{q,i,t}^{EV,D} + \sum_{m\in\Omega_b^M} \left(P_{m,i,t}^{S,D} - P_{m,i,t}^{S,C}\right) + \tag{2}$$

$$\sum_{l\in\Omega_{L_b}} P_{l,i,t}^L = P_{b,i,t}^D - P_{b,i,t}^S, \quad \forall b,i,t$$

$$u_{g,i,t} - u_{g,i',t+1} + u_{g,i'',t'} \geqslant 0, \quad 1 \leqslant t'-t \leqslant T_g^{on}, \quad \forall g,i,t \tag{3}$$

$$u_{g,i,t} - u_{g,i'',t+1} + u_{g,i'',t'} \leqslant 1, \quad 1 \leqslant t'-t \leqslant T_g^{off}, \quad \forall g,i,t \tag{4}$$

$$P_{g,i',t+1}^G - P_{g,i,t}^G \leqslant \left(2 - u_{g,i,t} - u_{g,i',t+1}\right)\underline{P}_g^G + \tag{5}$$

$$\left(1 + u_{g,i,t} - u_{g,i',t+1}\right)R_g^U, \quad \forall g,i,t$$

$$P_{g,i,t}^G - P_{g,i',t+1}^G \leqslant \left(2 - u_{g,i,t} - u_{g,i',t+1}\right)\underline{P}_g^G + \tag{6}$$

$$\left(1 - u_{g,i,t} + u_{g,i',t+1}\right)R_g^D, \quad \forall g,i,t$$

$$u_{g,i,t}\underline{P}_g^G \leqslant P_{g,i,t}^G \leqslant u_{g,i,t}\overline{P}_g^G, \quad \forall g,i,t \tag{7}$$

$$P_{l,i,t}^L - B_l\left(\theta_{b,i,t} - \theta_{b',i,t}\right) - M\left(1 - u_{l,i,t}^F\right) \leqslant 0, \quad \forall l,i,t \tag{8}$$

$$P_{l,i,t}^L - B_l\left(\theta_{b,i,t} - \theta_{b',i,t}\right) + M\left(1 - u_{l,i,t}^F\right) \geqslant 0, \quad \forall l,i,t \tag{9}$$

$$u_{l,i,t}^F\underline{P}_l^L \leqslant P_{l,i,t}^L \leqslant u_{l,i,t}^F\overline{P}_l^L, \quad \forall l,i,t \tag{10}$$

$$P_{G_{n,i,t}} - P_{D_{n,i,t}} = \sum_{m=1}^N (-B_{n,m})\theta_{m,i,t} \tag{11}$$

$$0 \leqslant P_{b,i,t}^S \leqslant P_{b,i,t}^D, \quad \forall b,i,t \tag{12}$$

$$\underline{\theta}_b \leqslant \theta_{b,i,t} \leqslant \overline{\theta}_b, \quad \forall b,i,t \tag{13}$$

Constraint (2) exhibits the power balance connection status of each node. The $P_{b,i,t}^D$ indicates the load requirement of node b in scenario i and at time t, and $P_{b,i,t}^S$ represents the load reduction in node b in the identical scenario and time. Ω_{L_b} and Ω_b^M, respectively, refer to the collection of transmission lines linked to node b and the set of associated energy storage devices. Constraint (3) establishes the minimum continuous operation time span of the generator. $u_{g,i,t}$ is a binary state variable of generator g at time t and in scenario i, where 1 indicates that the generator is operational, and 0 indicates that it is paused. T_g^{on} represents the minimum period within which the generator must maintain its operation once it has initiated. Constraint (4) claims that the generator must satisfy the requirement of minimum continuous down time. T_g^{off} represents the minimum continuous time within which the generator must remain out of operation once it has halted. Constraints (5) and (6) govern the ramp-up and ramp-down rates of the generator. R_g^U and R_g^D, respectively, represent the maximum ramp-up and ramp-down rates of generator g, with the aim of ensuring a smooth transition in power generation. Constraint (7) constrains the output power range of the generator. $\underline{P}_g^G$ and $\overline{P}_g^G$, respectively, signify the minimum and maximum output power limitations of generator g. Constraints (8) and (9) define the power flow and state limitations of the transmission line. B_l represents the admittance value of line l, and $\theta_{b,i,t}$ and $\theta_{b',i,t}$ represent the voltage phase angles at the nodes connected to line l in scenario i and at time t. $u_{l,i,t}^F$ is a binary variable utilized to represent the working status of line l, where 1 indicates the line is accessible, and 0 indicates it is inaccessible. Constraint (10) determines the power flow limit for each transmission line. The variables $\underline{P}_l^L$ and $\overline{P}_l^L$, respectively, represent the minimum and maximum power flow limits of transmission line l. Constraint (11) ensures the power balance at each node. $B_{n,m}$ represents the admittance value between node n and node m, and $\theta_{m,i,t}$ represents the voltage phase angle of node m in scenario i and at time t. Constraint (12) limits the load shedding to ensure that it does

not exceed the load demand. $P_{b,i,t}^S$ represents the load reductions, which must not exceed the load demand $P_{b,i,t}^D$. Constraint (13) limits the voltage phase angle range at each node. $\underline{\theta}_b$ and $\bar{\theta}_b$ represent the minimum and maximum voltage phase angles of node b, respectively.

4.2. Constraints on Energy Storage

$$SOC_{m,i,t}^S = SOC_{m,i,t-1}^S + \eta_m^C P_{m,i,t}^{S,C} - \frac{P_{m,i,t}^{S,D}}{\eta_m^D}, \quad \forall m,i,t \tag{14}$$

$$\underline{SOC}_m^S \leqslant SOC_{m,i,t}^S \leqslant \overline{SOC}_m^S, \quad \forall m,i,t \tag{15}$$

$$0 \leqslant P_{m,i,t}^{S,C} \leqslant u_{m,i,t}^{S,C} \overline{P}_m^S, \quad \forall m,i,t \tag{16}$$

$$0 \leqslant P_{m,i,t}^{S,D} \leqslant u_{m,i,t}^{S,D} \overline{P}_m^S, \quad \forall m,i,t \tag{17}$$

$$u_{m,i,t}^{S,C} + u_{m,i,t}^{S,D} \leqslant 1, \quad \forall m,i,t \tag{18}$$

Constraint (14) defines the State of Charge (SOC) dynamics of an energy storage system, including the effects of charging and discharging efficiency. Constraint (15) sets the upper and lower limits of SOC. Constraint (16) limits the charging power to the allowable range and is regulated by the charging state variable. Constraint (17) restricts the discharge power to the allowable range and is controlled by the discharge state variable. Constraint (18) ensures that the energy storage device can either be charged or discharged at any given time, but not both simultaneously.

4.3. Objective and Constraints of EV

The lower-level problem aims to maximize the discharge revenue for electric vehicle owners,

$$\max \quad \sum_{t \in T} \sum_{q \in \Omega_{EV}} C_{EV,D} P_{q,t}^{EV,D} \tag{19}$$

$$\text{s.t.} \quad SOC_{q,t}^{EV} = SOC_{q,t-1}^{EV} + \eta_q^{EV,C} P_{q,t-1}^{EV,C} - \frac{P_{q,t-1}^{EV,D}}{\eta_q^{EV,D}},$$

$$\forall q \in EVs, \ t > 0 \tag{20}$$

$$SOC_{q,0}^{EV} = SOC_{q,init}^{EV}, \quad \forall q \in EVs \tag{21}$$

$$SOC_{q,min}^{EV} \leq SOC_{q,t}^{EV} \leq SOC_{q,max}^{EV},$$

$$\forall q \in EVs, \ t \in T \tag{22}$$

$$P_{q,t}^{EV,C} \leq P_{q,max}^{EV} u_{q,t}^{EV,C}, \quad \forall q \in EVs, \ t \in T \tag{23}$$

$$P_{q,t}^{EV,D} \leq P_{q,max}^{EV} u_{q,t}^{EV,D}, \quad \forall q \in EVs, \ t \in T \tag{24}$$

$$u_{q,t}^{EV,C} + u_{q,t}^{EV,D} \leq 1, \quad \forall q \in EVs, \ t \in T \tag{25}$$

The objective function is presented in constraint Condition (19) to maximize the total discharge benefits of electric vehicles (EVs) over the planning cycle and to maximize their economic potential. Constraint Condition (20) describes the change of state of charge (SOC) of an EV energy storage system, taking into account the effect of charge and discharge efficiency. Constraint (21) defines the initial SOC state. Constraint (22) sets the upper and lower limits of SOC. Constraints (23) and (24) limit the charging and discharging power of EV, respectively. Constraint (25) ensures that electric vehicles can only choose one operation during charging or discharging at any time, avoiding simultaneous operations.

The upper-level problem minimizes the total operating costs of the power system, while the lower-level problem maximizes the benefits for EV owners. By iteratively solving

the bi-level optimization problem, the balance between the system cost and the benefit of electric vehicle owners is realized.

5. Case Studies

Due to the lack of public data sets on power grid operation under extreme typhoon conditions, this study adopts Monte Carlo simulation method to simulate the influence of typhoon on a custom radial structure 57-node power system based on the line failure probability model [22] under typhoon scenarios. The specific data generation and optimization model flow of this paper is as follows. Following the modeling methods in [22], a 24-h typhoon event is simulated to generate training and testing datasets. The study aims to minimize load loss and total system operational costs by designing a scheduling strategy that integrates prediction and optimization. In this paper, we construct a power system with a radial topology that integrates a custom-designed energy storage unit and an electric vehicle (EV) node. The key parameters of the system are adjusted according to the actual typhoon disaster scenario.

The Batts typhoon wind field model is used to calculate the real-time wind speed across transmission lines within the affected area. Combining the wind speed with the failure probability model for transmission lines, state data of the lines are generated. Using multivariate Monte Carlo simulations, key factors such as line geographic location, design wind speed, typhoon path, and distance from the typhoon center are considered to produce a large-scale, scenario-encompassing dataset.

A Transformer-based prediction model is implemented using Python. By leveraging self-attention mechanisms, the model captures temporal dependencies among input features, predicts the operational status (operational or failed) of transmission lines under typhoon conditions, and provides high-accuracy results.

Based on the prediction results, a bi-level optimization problem is solved using the Gurobi optimizer, where the upper-level model aims to minimize total system operational costs, including generation costs, load loss costs, and other related expenses, while the lower-level model focuses on maximizing the economic benefits of EV users. These two models are interconnected through shared decision variables, ensuring that the prediction results are seamlessly integrated into the optimization-based scheduling process.

In this study, the SPO framework is used to dynamically adjust the prediction model parameters by minimizing the SPO loss function using the difference between the scheduling cost caused by the prediction error and the optimal cost as feedback. This ensures that the prediction results are consistent with the optimization objective, thus improving the decision quality. In the cross-entropy method, the model only focuses on the accuracy of the predicted line state, but ignores how the prediction results affect the final scheduling decision. However, in the SPO method, the accuracy of the line state is only an intermediate link, and the ultimate goal is to reduce the system cost through effective scheduling optimization. Compared with the traditional cross-entropy loss method, the SPO framework solves the problem of the separation of the prediction and scheduling modules of the cross-entropy method in the environment without cost feedback by integrating the negative cost feedback into the prediction and optimal scheduling process. Therefore, the SPO method not only focuses on the accuracy of the line state, but also considers optimizing the decision results to better enhance the system performance.

5.1. Results Analysis

During typhoon simulations, a straight-line path is assumed for the typhoon's motion. The real-time status of transmission lines is calculated at multiple time steps. At each time

step, line statuses are provided by the prediction model, which are then used to update the scheduling plan dynamically, achieving real-time decision-making.

This section compares the performance of the Cross-Entropy Loss method and the SPO method in terms of line status prediction accuracy, total cost, and load shedding. The results show that even with similar prediction accuracy, the SPO method achieves superior cost control and load management. The SPO method effectively leverages prediction outcomes to achieve better system performance in subsequent dispatch optimizations, demonstrating its capacity to provide robust decision support under limited prediction accuracy.

We conducted a comparison between the SPO loss function as the experimental group and the cross-entropy loss function as the control group. According to Table 1 data, the accuracy rate of the experimental group was considerably higher than that of the control group even after only one training epoch. Based on the confusion matrix data of the experimental group, it was found that the accuracy rate of the experimental group typically exceeded 97%, while that of the control group was generally around 60% in the first epoch. Nevertheless, by the seventh training epoch, the accuracy rates of both groups were upper 97%.

Table 1. Confusion matrices for Control and Experimental groups at Epochs 1 and 4 for power grid line statuses.

		Epoch 1—Control Group	
		Predicted	
		Operational	**Outage**
Actual	**Operational**	0.6484	0.3516
	Outage	0.3430	0.6570
		Epoch 1—Experimental Group	
		Predicted	
		Operational	**Outage**
Actual	**Operational**	0.9970	0.0030
	Outage	0.0240	0.9760
		Epoch 7—Control Group	
		Predicted	
		Operational	**Outage**
Actual	**Operational**	0.9933	0.0067
	Outage	0.0145	0.9855
		Epoch 7—Experimental Group	
		Predicted	
		Operational	**Outage**
Actual	**Operational**	0.9978	0.0022
	Outage	0.0247	0.9753

At the same time, we chose the prediction accuracy rate data for damaged lines and made Figure 2. From the figure, it can be seen that there was a significant difference in the accuracy rate between the control group and the experimental group in the first two epochs. The accuracy rate of the control group was only about 65.7% in the first and second epochs, but it rose rapidly to 97.8% in the third epoch, reached a peak of nearly 99.7% in the fourth epoch, and declined slightly to about 98.3% in the fifth epoch. In contrast, the

accuracy rate of the experimental group was as high as 97.8% in the first epoch, but was surpassed by the control group in the third epoch, and then fluctuated steadily without further improvement in the following epochs.
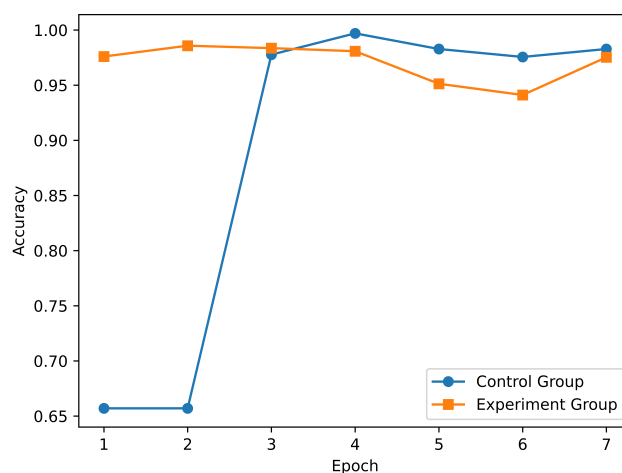

Figure 2. Accuracy comparison between Experimental and Control groups.

In conclusion, the experimental group exhibited a faster convergence rate, significantly outperformed the control group in terms of accuracy rate in the early epochs, and demonstrated more stable performance. This indicates that the optimization method of the experimental group not only possesses a higher accuracy rate, but also significantly reduces training time and has higher practicality. To sum up, the experimental group manifested faster convergence, saved training time and computing resources, and provided better real-time response capabilities in practical applications.

5.2. Cost Comparison

Under extreme weather conditions, even with similar accuracy in predicting grid line statuses, the SPO method still significantly reduces total system costs. The comparison is presented in Table 2.

Table 2. Total cost comparison across different groups and epochs.

Comparison Item	Total Cost (CNY)
Epoch 1 Control Group Total Cost	24,750,096.35
Epoch 7 Control Group Total Cost	25,602,191.73
Epoch 1 Experimental Group Total Cost	10,332,719.38
Epoch 7 Experimental Group Total Cost	9,056,648.69

As seen in Table 2, the total cost achieved by the experimental group after training for only one epoch is still much better than that of the control group trained for seven epochs. The total cost of the experimental group Epoch 1 decreased by 59.63% compared to the total cost of the control group Epoch 7. In addition, by increasing the number of training epochs for the experimental group, we can see that the total cost of the experimental group in Epoch 7 is further reduced by 12.35% compared to the total cost of the experimental group in Epoch 1. This shows that the SPO loss function can achieve significant results even in the first round. Although the prediction accuracy of the control group has improved greatly after seven epochs, the cost has not changed significantly, but increased slightly by 3.44%. It can be seen that the cost of the ordinary cross-entropy function may not be significantly improved after the prediction accuracy is greatly improved.

It can be seen from Figure 3 that high prediction accuracy does not necessarily directly translate into the optimal decision scheduling effect. Throughout all training rounds, the total cost of the experimental group was consistently significantly lower than that of the control group. This is due to the SPO optimization framework embedding the decision scheduling objective function directly into the prediction module, effectively integrating the prediction results with the optimization goal and significantly enhancing the effectiveness of the scheduling decision and its practical application value.
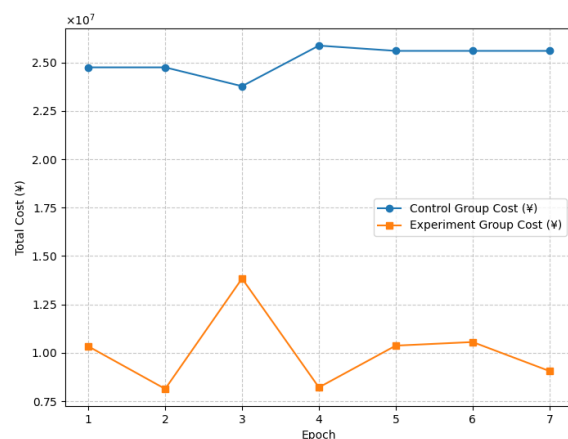
Figure 3. Comparison of Costs between Experimental and Control groups.

5.3. Load Shedding Comparison

The SPO approach shows superior flexibility in load management. Even in the case of similar prediction accuracy, load loss can still be greatly improved by scheduling generation units, energy storage and EV scheduling. Its load reduction is much less than that of the comparison group using the cross-entropy function, as follows.

In this study, in order to ensure the resilience of the power system under typhoon condition, I set a high unit cost of load reduction losses. The goal is to allow the system to prioritize system stability and resource allocation in the face of load reduction. At the same time, by increasing the unit cost of load reduction, the optimization model is forced to avoid large-scale load reduction when scheduling, so as to ensure the robustness of the system to the maximum extent. The optimization process is completed by Gurobi solver. The model takes into account the limit of generator climbing power, line disconnection and other system instability factors to ensure the rationality and practicability of scheduling results.

Table 3 and Figure 4 summarize the load reduction and cost changes in the experimental group compared with the control group. The total load reduction for the control group in the first cycle was 24,748.45 kW as the baseline data. In the seventh cycle, the total load reduction in the control group increased to 25,600.32 kW, which is 3.44% higher than in the first cycle.

Table 3. Total load shedding and cost changes compared to Control group.

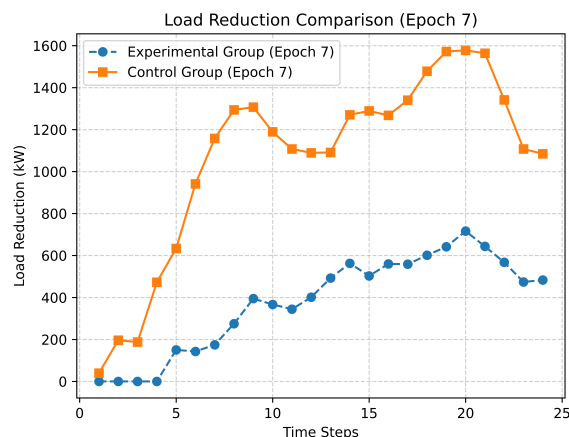| Group	Total Load Shedding (kW)	Cost Change Compared to Control (%)
Epoch 1 Control	24,748.45	-
Epoch 7 Control	25,600.32	3.44%
Epoch 1 Experimental	10,329.75	−58.26%
Epoch 7 Experimental	9053.49	−63.42%

Figure 4. Comparison of load reduction between Experimental and Control groups.

In contrast, the experimental group had a total load reduction of 10,329.75kW in the first cycle, a reduction of 58.26% compared to the control group. In the seventh cycle, the total load reduction in the experimental group was further reduced to 9053.49 kW, 63.42% lower than that of the control group.

This shows that when the control group and the experimental group have similar prediction accuracy, the SPO method can make more effective decisions and significantly reduce load shedding by using cost as a negative feedback. By setting a higher unit cost of load reduction loss in the experimental group, the system can focus more on load reduction in the optimization process on the basis of ensuring toughness, thus achieving better scheduling results, reducing load reduction and effectively controlling the total system cost.

6. Conclusions

In this paper, a bi-level optimization model based on the SPO framework is proposed to deal with the challenges of power grid scheduling under extreme weather conditions. By combining prediction and optimization, the SPO method can rapidly respond to and optimize power system resource scheduling in the face of complex and dynamically changing extreme weather events, thereby effectively reducing load reduction and total system costs. Specifically, this paper first uses the Transformer-based prediction model to predict the real-time damage state of transmission lines in the power system, and then dynamically dispatches power grid resources through the bi-level optimization model. The upper-level model aims to minimize the overall cost of the power system, covering generation costs, load loss costs, etc., while the lower-level model focuses on maximizing the economic benefits for electric vehicle (EV) owners.

The research results show that the SPO method can not only effectively reduce the total cost and load reduction in the system on the basis of ensuring high forecasting accuracy, but also show significant advantages in cost control and load management under similar forecasting accuracy conditions. Through comparative experiments, the SPO method can realize more optimized resource allocation under the condition of limited resources and limited prediction accuracy, thus improving the system economy and enhancing the robustness and adaptability of the system. This shows that the SPO method can provide effective decision support for power grid dispatching under uncertain environments, such as extreme weather.

However, there are some limitations to this study. First, of all, the assumption of the typhoon path adopted in this paper is a straight line, without considering the complex changes of the typhoon path. In the future, a more complex typhoon path model can be introduced to improve the applicability of the model. Secondly, this study mainly

focuses on the typhoon weather scenario, which can be extended to other types of extreme weather events such as heavy rain and drought in the future to enhance the universality and practicability of the model. In addition, the current bi-level optimization model adopts DC power flow constraints and does not consider the influence of reactive power on the system. Future studies could consider using AC power flow constraints and incorporate reactive power to further analyze the system's stability.

In conclusion, this research provides an innovative solution for power grid dispatch under extreme weather conditions. By combining efficient prediction with optimization, the SPO framework not only improves the efficiency and economy of grid scheduling but also provides theoretical support and practical guidance for future responses to complex and changing extreme weather events.

References

1. Panteli, M.; Mancarella, P. Influence of extreme weather and climate change on the resilience of power systems: Impacts and possible mitigation strategies. *Electr. Power Syst. Res.* **2015**, *127*, 259–270.
2. Jun, G.; Feng, T.; Zelin, C.; Xianglong, L.; Wenhu, T. Vulnerability assessment for power transmission lines under typhoon weather based on a cascading failure state transition diagram. *Energies* **2020**, *13*, 3681.
3. Watson, E.B.; Etemadi, A.H. Modeling electrical grid resilience under hurricane wind conditions with increased solar and wind power generation. *IEEE Trans. Power Syst.* **2019**, *35*, 929–937.
4. Salman, A.M.; Li, Y.; Stewart, M.G. Evaluating system reliability and targeted hardening strategies of power distribution systems subjected to hurricanes. *Reliab. Eng. Syst. Saf.* **2015**, *144*, 319–333.
5. Tari, A.N.; Sepasian, M.S.; Kenari, M.T. Resilience assessment and improvement of distribution networks against extreme weather events. *Int. J. Electr. Power Energy Syst.* **2021**, *125*, 106414.
6. Chang, L.; Wu, Z. Performance and reliability of electrical power grids under cascading failures. *Int. J. Electr. Power Energy Syst.* **2011**, *33*, 1410–1419.
7. Lian, X.; Qian, T.; Li, Z.; Chen, X.; Tang, W. Resilience assessment for power system based on cascading failure graph under disturbances caused by extreme weather events. *Int. J. Electr. Power Energy Syst.* **2023**, *145*, 108616.
8. Hou, H.; Geng, H.; Huang, Y.; Wu, H.; Wu, X.; Yu, S. Damage probability assessment of transmission line-tower system under typhoon disaster, based on model-driven and data-driven views. *Energies* **2019**, *12*, 1447.
9. Yu, Q.; Li, Z.; Han, X.; Ju, P.; Shahidehpour, M. End-to-end learning for stochastic preventive dispatch of renewables-rich power systems in abnormal weather conditions. *Renew. Energy* **2024**, *234*, 121107.
10. Li, R.; Zhang, H.; Sun, M.; Teng, F.; Wan, C.; Pineda, S.; Kariniotakis, G. Decision-oriented learning for future power system decision-making under uncertainty. *arXiv* **2024**, arXiv:2401.03680.
11. Wahdany, D.; Schmitt, C.; Cremer, J.L. More than accuracy: End-to-end wind power forecasting that optimises the energy system. *Electr. Power Syst. Res.* **2023**, *221*, 109384.
12. Elmachtoub, A.N.; Grigas, P. Smart "predict, then optimize". *Manag. Sci.* **2022**, *68*, 9–26.
13. Eskandarpour, R.; Khodaei, A.; Paaso, A.; Abdullah, N.M. Artificial intelligence assisted power grid hardening in response to extreme weather events. *arXiv* **2018**, arXiv:1810.02866.
14. Zhang, J.; Wei, J.; Li, X. Impact analysis of typhoon on cascading failure for electric power system. *Electr. Power Autom. Equip.* **2019**, *39*, 157–162.
15. Wang, Z.; Wang, Z. A novel preventive islanding scheme of power system under extreme typhoon events. *Int. J. Electr. Power Energy Syst.* **2023**, *147*, 108857.

16. Hou, H.; Yu, S.; Wang, H.; Xu, Y.; Xiao, X.; Huang, Y.; Wu, X. A hybrid prediction model for damage warning of power transmission line under typhoon disaster. *IEEE Access* **2020**, *8*, 85038–85050.

17. Dai, Z. Transformer-xl: Attentive language models beyond a fixed-length context. *arXiv* **2019**, arXiv:1901.02860.

18. Javadi, E.A.; Joorabian, M.; Barati, H. A bi-level optimization framework for resilience enhancement of electricity and natural gas networks with participation of energy hubs. *Int. J. Electr. Power Energy Syst.* **2022**, *142*, 108312.

19. Fan, W.; Tan, Q.; Zhang, A.; Ju, L.; Wang, Y.; Yin, Z.; Li, X. A Bi-level optimization model of integrated energy system considering wind power uncertainty. *Renewable Energy* **2023**, *202*, 973–991.

20. Liu, W.; Fu, M.; Yang, M.; Yang, Y.; Wang, L.; Wang, R.; Zhao, T. A bi-level interval robust optimization model for service restoration in flexible distribution networks. *IEEE Trans. Power Syst.* **2020**, *36*, 1843–1855.

21. Qiu, H.; Zhao, B.; Gu, W.; Bo, R. Bi-level two-stage robust optimal scheduling for AC/DC hybrid multi-microgrids. *IEEE Trans. Smart Grid* **2018**, *9*, 5455–5466.

22. Liu, X.; Hou, K.; Jia, H.; Zhao, J.; Mili, L.; Jin, X.; Wang, D. A planning-oriented resilience assessment framework for transmission systems under typhoon disasters. *IEEE Trans. Smart Grid* **2020**, *11*, 5431–5441.